frontiers | Frontiers in Climate

TYPE Original Research
PUBLISHED 25 November 2025
DOI 10.3389/fclim.2025.1656283

OPEN ACCESS

EDITED BY
Matthew Collins,
University of Exeter, United Kingdom

REVIEWED BY
Daniel Gebregiorgis,
Georgia State University, United States
Daris Correia Dos Santos,
Federal University of Rio Grande do Norte, Brazil

*CORRESPONDENCE
Rosimeire Araújo Silva
✉ cientistadedados@gmail.com

RECEIVED 29 June 2025
ACCEPTED 28 October 2025
PUBLISHED 25 November 2025

CITATION
Silva RA and Fearnside PM (2025) The roots of Amazonia's droughts and floods: complex interactions of Pacific and Atlantic sea-surface temperatures.
Front. Clim. 7:1656283.
doi: 10.3389/fclim.2025.1656283

The roots of Amazonia's droughts and floods: complex interactions of Pacific and Atlantic sea-surface temperatures

Rosimeire Araújo Silva* and Philip Martin Fearnside

Instituto Nacional de Pesquisas da Amazônia, INPA, Manaus, Amazonas, Brazil

The relationship between sea surface temperatures (SST) and climate events in the Amazon is more complex than suggested by traditional climate models, involving the of multiple oceanic drivers and spatially and temporally heterogeneous responses across the basin. The first EOF mode in the tropical Pacific corresponds to Central El Niño events, featuring basin-wide positive SST anomalies with 2 to 8 year cycles. The second mode relates to Eastern El Niño events, showing localized positive anomalies in the Niño 1 + 2 region and opposing negative anomalies in northern and southern Pacific, with shorter 1 to 4 year oscillations. In the tropical Atlantic, the main EOF mode is the Equatorial Atlantic Mode (EAM), characterized by basin-wide negative SST anomalies on 2 to 4 year cycles. The second Atlantic mode is the Positive Atlantic Dipole, distinguished by opposing SST anomalies in the northern and southern tropics, varying between 6 months and 1 year. Correlation analyses between these climate modes and the Palmer Drought Severity Index (PDSI) show that Central El Niño strongly influences Amazon droughts year-round, especially in northern and central sub-basins like Japurá, Negro, Trombetas-Uatumã, and Paru-Jari. The impact of the Eastern El Niño is milder and spatially heterogeneous, with opposite effects particularly evident in the Upper Negro sub-basin. The cold phase of the EAM favors wetter rainy seasons but can induce moisture reduction during the transition to the dry season, especially when combined with other seasonal forcings. When the Positive Atlantic Dipole occurs in the rainy season, Japurá and Negro basins become wetter, but other sub-basins face moderate drought. This oceanic pattern promotes drier conditions, bringing forward the onset of the dry season in practically all sub-basins. Our results demonstrate that Pacific and Atlantic oceanic patterns play complementary roles, with Central El Niño driving widespread and prolonged droughts, while Atlantic modes modulate the of extreme events, often amplifying or attenuating the impacts depending on the sub-basin considered. This enhanced understanding of coupled ocean–atmosphere interactions is essential for improving climate prediction, water resource management, and adaptation strategies in the face of increasing hydroclimatic extremes in the Amazon Basin.

KEYWORDS

Amazon sub-basins, climate, ENSO, Atlantic dipole, Atlantic Equatorial Mode, hydroclimate

1 Introduction

In recent years, the Amazon has faced a significant increase in frequency of extreme weather events, such as droughts and floods, which highlights the importance of understanding the roots of these events (Garcia et al., 2018; Espinoza et al., 2019, 2022). Severe droughts in the northern portion of the Amazon are generally triggered by El Niño, while droughts in the

southern portion appear to be more controlled by tropical Atlantic warming (e.g., Espinoza et al., 2019). The 2015–16 El Niño differed from other events, with the effect also extending to the southern part of the Amazon, affecting the state of Acre (Silva et al., 2018). Droughts in the southwestern Amazon caused by warming sea surface temperature in the tropical North Atlantic, as in 2005 and 2010, are exacerbated if this warming is in combination with a cooling in the tropical South Atlantic (Cox et al., 2008).

Climate models indicate a high chance that the coming decades will have El Niño events with unprecedented intensities (Latif et al., 2015), and that there will be unprecedented droughts in the Brazilian Amazon (Kay et al., 2022). In relation to the historical average, the probability of severe droughts in Brazil is forecast to increase by a factor of four under a mean global temperature 1.5 °C above the pre-industrial level and by a factor of ten under a mean global temperature 4 °C above this average (Price et al., 2022). Clearly, it is urgent to have the best possible understanding of the relations between extreme weather events in the Amazon and the tropical oceanic patterns impacted by global warming.

Interannual variability of rainfall in the Amazon is associated with the El Niño Southern Oscillation (ENSO) phenomenon (Kayano and Andreoli, 2006; Araújo et al., 2013), that is, El Niño events (positive SST anomalies) and La Niña events (negative SST anomalies) in the tropical Pacific, producing large-scale anomalous circulation events in the atmosphere that generate significant impacts across South America (Aceituno, 1988; Grimm et al., 1998; Grimm and Zilli, 2009). Rainfall in the Amazon exhibits great interannual and decadal variability, which has been attributed to variations in the surface temperatures (SST) in both the tropical Pacific and Atlantic Oceans (Ronchail et al., 2002; Marengo, 2004; Ronchail and Gallaire, 2006; Zeng et al., 2008). ENSO contributes significantly to the variability of the Atlantic SST and most Atlantic SST anomalies are linked to ENSO in the Pacific (Enfield and Mayer, 1997; Giannini et al., 2000; Czaja et al., 2002; Guan and Nigam, 2009). Tropical Atlantic variability can play a role in preconditioning the teleconnection between ENSO and rainfall in Brazil (Giannini et al., 2004).

The study by Zhao and Capotondi (2024) underscores the crucial role of coupled Atlantic–Pacific interactions in modulating tropical Pacific variability and its global implications across interannual to decadal timescales. Employing a Linear Inverse Model (LIM) calibrated with observational data, the authors systematically evaluated the bidirectional influences between the Atlantic and Pacific Oceans. Their results indicate that internal variability in the Atlantic enhances interannual SST anomalies in the eastern equatorial Pacific and decadal SST anomalies in the central equatorial Pacific. In contrast, feedbacks from the Pacific to the Atlantic act to suppress decadal variability in the tropical Pacific. This methodological approach also provides a useful framework for assessing the performance of climate models in representing cross-basin interactions.

In years with warm water in the central equatorial Pacific, the Intertropical Convergence Zone (ITCZ) is found anomalously further north of its position over the Atlantic Ocean, and the northeast trade winds are weakened, reducing moisture transport to the interior of the Amazon region (Marengo and Hastenrath, 1993; Marengo, 2005). In El Niño years in the 1979–2000 period there were reductions in precipitation, runoff, and the convergence of humidity, while in La Niña years these measurers had above-average values (Marengo, 2006).

Yoon and Zeng (2010) found that only a fraction of the rainfall variability in the Amazon can be explained by ENSO, and that this relationship is only active during the rainy season. These authors suggested that the influence of the tropical North Atlantic on climate variability in the Amazon region can be comparable to the best-known teleconnections with ENSO from the Pacific Ocean, agreeing with previous studies that have shown Amazonian precipitation variations to also be related to SSTs in the Atlantic (Liebmann and Marengo, 2001; Marengo et al., 2008).

The potential influence of the tropical Atlantic on rainfall patterns in the Amazon region gained prominence following a severe drought in 2005, a notable event documented by Marengo et al. (2008) and Zeng et al. (2008). This drought was one of the most severe in a century, with significant repercussions on Amazonian tributaries like the Solimões and the Madeira in the southern Amazon (Marengo et al., 2008). While the drought's impact was pronounced in these southern regions, there were no substantial alterations in rainfall or river levels observed in the northeastern Amazon, which had previously experienced severe droughts during extreme El Niño events in 1926, 1983, and 1998. The anomalous drought of 2005 prompted a deeper investigation into the potential influence of Atlantic SST on the Amazon's climate dynamics and the respective roles of the Pacific and Atlantic Oceans.

Handoh et al. (2006) investigated the relationships between SST variability in the tropical North Atlantic and anomalous events in the Pacific and proposed that ENSO events induce wind and latent heat flux anomalies over the tropical Atlantic, and that a considerable portion of the interannual variability in tropical North Atlantic SSTs can be explained by teleconnections associated with ENSO. However, Lee et al. (2008) showed that not all ENSO events can guarantee a tropical North Atlantic SST warmer than the climatological average, showing that the temporal evolution of an ENSO event is crucial to define a warming or cooling in the Atlantic, and that such relationships are explained by means of an extratropical wave train from the Pacific.

A relationship seems to exist between SST variability in the tropical Pacific and Atlantic Oceans and the atmospheric system, and the result of this interaction is coupled to the overlying atmospheric wind. The Walker circulation is a mechanism linking anomalously warm Pacific SST with dry conditions in the Amazon basin (Marengo and Hastenrath, 1993). The anomalous circulation pattern during a hot episode is associated with an eastward shift of the Walker circulation, with an ascendant movement positioned in the central and eastern equatorial Pacific due to the strong convection established by warmer waters and subsidence movement of air in other locations, including the North and Northeast Regions of Brazil. The strengthening of the jet is due to warming in the equatorial Pacific, which causes a strengthening of the north–south temperature gradient and also transports latent heat at high levels in the tropics by the westerly winds (Bjerknes, 1966, 1969). As a result, the normal rainfall pattern over the tropical belt is modified. Rainfall below the climatological normal is noted in the North and Northeast Regions of Brazil, while the South and Southeast Regions experience above-normal rainfall (Ropelewski and Halpert, 1989).

There are two types of El Niño event: the central Pacific El Niño (or "modoki" El Niño) and the eastern Pacific El Niño or "canonical El Niño" (Ashok et al., 2007). Kao and Yu (2009) examined the modes separately using a method that combined Empirical Orthogonal Functions (EOF) and linear regression. The central El Niño is characterized by positive SST anomalies confined to the central equatorial Pacific (Kao and Yu, 2009; Feng et al., 2020), while the eastern El Niño is associated with a westward spread of positive SST

anomalies from the coast of South America in the eastern equatorial Pacific (Rasmusson and Carpenter, 1983). This spatial variability implies different convection patterns and atmospheric responses to warming that can produce different climate teleconnections across the globe (Ashok et al., 2007; Takahashi et al., 2011).

This study explores the complex interplay between SST anomalies in the tropical Pacific and Atlantic Oceans and the occurrence of droughts and floods in the Amazon between 1950 and 2022. Using the EOF method, the main modes of climate variability—Central El Niño, Eastern El Niño, Equatorial Atlantic Mode (EAM), and Atlantic Dipole—were identified. By analyzing correlations with the Palmer Drought Severity Index (PDSI), the study assesses how these modes influence Amazonian sub-basins over time and space, highlighting the distinct and complementary roles of the Pacific and Atlantic in shaping regional hydroclimate variability.

2 Materials and methods

2.1 Study area

The Amazon Basin is the largest tropical river basin in the world, covering approximately 6.9 million km^2 and encompassing several countries in South America. According to Feldpausch et al. (2012), it is characterized by a vast and dense tropical forest, a complex hydrographic network, and significant spatial variability in topography and hydrological conditions, as highlighted by Sioli (1984). The region's climate is predominantly equatorial, with high humidity and annual precipitation ranging from 1,500 to over 3,000 mm, with well-defined rainy and dry seasons depending on the sub-basin and local topography (Salati and Vose, 1984).

The Amazon basin has been divided into nine main sub-basins, each exhibiting distinct hydrological and climatic characteristics. In this study, we focus on the Japurá, Negro, Trombetas–Uatumã, Paru–Jari, Javari–Juruá, Purus, Madeira, Tapajós, and Xingu sub-basins, as shown in Figure 1. These sub-basins cover a wide latitudinal and longitudinal gradient, encompassing areas with contrasting precipitation patterns and hydrological regimes. The Central Amazon region is highlighted with a red "X" to indicate the location of the ANA hydrological station in Manaus, which serves as a key reference for river level monitoring and hydrological analysis.

This spatial framework allows for detailed investigation of oceanic climate mode influences (e.g., ENSO, EeamAM, Atlantic Dipole) on droughts and floods, capturing heterogeneous responses among sub-basins and providing operationally relevant insights for hydrological monitoring and early warning systems.

2.2 Sea surface temperature (SST)

The SST data consist of a reconstructed global monthly series for each grid point, with spatial resolution of 2° latitude by 2° longitude

FIGURE 1
Sub-basins of the Amazon Basin: the map highlights the main sub-basins, including the Japurá River sub-basin, Rio Negro sub-basin, Jatapu River sub-basin, Trombetas River sub-basin, Jutaí River sub-basin, Purus River sub-basin, Madeira River sub-basin, Tapajós River sub-basin, and Xingu River sub-basin. The central Amazon region is marked with a red "X," emphasizing the location of the ANA hydrological station in Manaus.

(Smith et al., 2008). These data are available at https://psl.noaa.gov/data/gridded/data.noaa.ersst.v5.html for the period from 1950 to 2022.

2.3 Palmer drought severity index (PDSI)

The Palmer Drought Severity Index (PDSI) is a widely used climatic index designed to quantify the severity and duration of droughts and wet periods by assessing soil moisture anomalies. Developed by Wayne Palmer in 1965, the index integrates monthly temperature and precipitation data with soil water-holding capacity, enabling it to reflect deviations from normal moisture conditions relative to local climatology.

This study employs the self-calibrated Palmer Drought Severity Index (scPDSI), which improves upon the original PDSI by dynamically calibrating its parameters to local climate variability, enhancing accuracy across diverse climatic regions (Wells et al., 2004). The scPDSI accounts for regional differences in moisture availability and evapotranspiration, making it particularly suitable for heterogeneous biomes such as the Amazon.

The dataset used is provided by the NOAA Physical Sciences Laboratory (PSL) and covers the global land surface from 1948 to 2014, with a spatial resolution of 2.5° x 2.5°. This long-term monthly series enables robust trend analyses and characterization of hydroclimatic variability over decadal timescales. The self-calibrated dataset is publicly available at: https://psl.noaa.gov/data/gridded/data.pdsi.html. PDSI values are standardized so that negative values indicate drought severity (with values below −4 representing extreme drought), and positive values indicate increasingly wet conditions.

The scPDSI has been extensively applied in hydrological and climate studies worldwide, including investigations of drought trends and impacts in tropical regions, providing a reliable metric for monitoring moisture deficits and excesses relevant to ecosystem and water resource management.

2.4 Water levels in Central Amazonia

The Manaus fluviometric station, identified by code 14990000, has been monitoring water levels of the Rio Negro in the Manaus region from 1903 to the present. The data collected by this station are provided by the Brazilian National Water and Basic Sanitation Agency (ANA) through the Hidroweb system, available at: https://www.snirh.gov.br/hidroweb/serieshistoricas. These historical records are essential for hydrological analyses, water resource management, and studies related to extreme events such as floods and droughts in the Central Amazon region. A station Manaus was selected due to its central geographic location within the Amazon Basin. Positioned at the confluence of major sub-basins in the lower Rio Negro region, it serves as a hydrological integrator. Typically, when low water levels are observed at this station, drought conditions are already affecting many upstream tributaries. Therefore, this central station offers a reliable proxy for broader basin-scale drought assessment.

2.5 Analysis methodology

To select the dominant modes of variability in the tropical Pacific and Atlantic, Empirical Orthogonal Functions (EOF) were applied to total SST anomalies in the tropical Pacific (180°–80°W; 20°S–20°N) and tropical Atlantic (70°W–10°E; 20°S–20°N) for the period from 1950 to 2022. EOF is a useful tool for identifying the principal modes of temporal and spatial variability in a given region. A key aspect in EOF analysis is the identification of statistically independent modes; according to the criterion proposed by North et al. (1982), a mode can be considered physically independent if its associated eigenvalue is well separated from the subsequent ones. In this study, the first two EOF modes in each basin meet this criterion. The associated principal components (PCs), also known as expansion coefficients, are normalized time series that describe the temporal evolution of the spatial patterns.

The methodology of this study adopts a statistical approach to investigate the relationship between climate patterns and drought severity in the Amazon region, using EOF analysis. The EOF technique is applied to reduce the dimensionality of the climate datasets and to identify the main modes of variability, extracting the dominant patterns that account for most of the observed variability. In this study, the first two EOF modes are associated with Pacific climate patterns—such as Central El Niño and Eastern El Niño—and Atlantic modes—such as the Equatorial Atlantic Mode (EAM) and the Atlantic Dipole.

The spectrum of each selected principal component (PC) was examined through Wavelet Transformation. The Morlet wavelet is particularly suitable for SST variability studies, as its oscillatory pattern resembles that of sea surface temperature fluctuations (Torrence and Compo, 1998). In addition to the normalized series, we present the dominant variability scales along with local and global power spectra for each pair of oceanic PCs.

Spatial correlation analysis was employed to assess the relationship between the climate modes identified by EOF and the PDSI in the Amazon. This technique helps identify areas within the Amazon Basin that are more sensitive to large-scale oceanic variability, offering a clearer picture of regional impacts associated with climate anomalies. The contributions of each oceanic mode are distinct, and the correlation between the PCs and the PDSI highlights which aspects of each mode are more closely linked to drought or increased moisture in specific regions. The PDSI integrates monthly temperature and precipitation data, along with soil water holding capacity, thereby enabling a robust assessment of how variability in oceanic modes translates into climate anomalies at the land surface.

The study also investigates the monthly PC anomaly fluctuations during years of extreme hydrological events in Central Amazonia. Historical river level data from the Manaus gauge station on the Lower Negro River sub-basin (provided by ANA) were used to represent the central region of the basin and to identify years with the most severe drought and flood events. The analysis of monthly anomalies enables the identification of SST variations during key periods leading up to the peaks of local droughts and floods.

In summary, this methodology integrates statistical techniques—including the correlation of oceanic PCs with the PDSI—to explore how and when Pacific and Atlantic climate patterns influence extreme events in the Amazon. The inclusion of hydrological data from Central Amazonia, in combination with historical climatological context, is critical for identifying local events and understanding their real-world impacts in the region.

3 Results

3.1 Tropical Pacific Ocean

The results presented here refer to the EOF analysis and their corresponding PCs for the Tropical Pacific region, highlighting dominant climate variability patterns. The first mode, which explains 53.9% of the total variance, shows a broad positive anomaly covering a large portion of the Tropical Pacific (Figure 2a). The most intense anomalies are centered over the central Pacific, particularly between 150°W and 120°W. This pattern is characteristic of warming events such as El Niño, marked by abnormally warm sea surface temperatures in the central Pacific basin.

The first Principal Component (PC1), associated with Mode 1 (Figure 2b), illustrates the temporal evolution of this pattern between 1950 and 2022. A clear alternation between positive and negative phases is observed, reflecting typical El Niño (positive peaks) and La Niña (negative trough) events.

Strong Central El Niño events, such as those observed in 1957–58, 1972–73, 1982–83, 1997–98, and 2015–16, stand out as positive peaks in PC1. In contrast, negative phases indicate the occurrence of La Niña events, including 1956–57, 1976–77, 1987–88, 2007–08, 2011–12, and 2021–22. This temporal pattern highlights the importance of interannual variability associated with the ENSO, the primary driver of climate anomalies in the tropical Pacific region.

The second mode (Mode 2), shown in Figure 2c and explaining 13.3% of the variance, reveals a dipole pattern with negative anomalies in the western Pacific and positive anomalies in the eastern sector, between 120°W and 90°W. This structure is characteristic of Eastern Pacific El Niño events, marked by alternating warming and cooling phases in that region. The associated PC2 exhibits smaller amplitudes

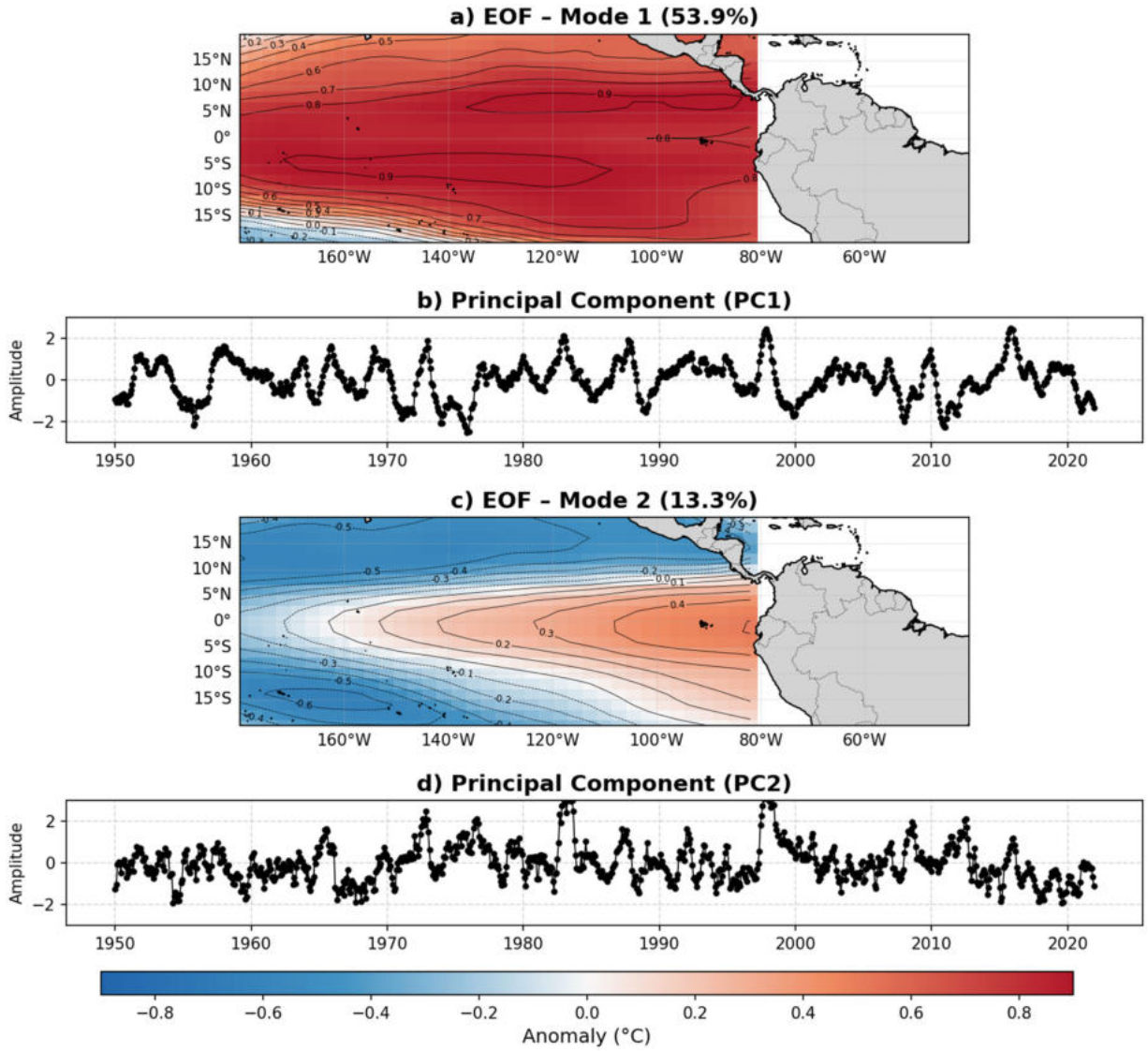

FIGURE 2
Empirical orthogonal function (EOF)—tropical Pacific. **(a)** Mode 1 (53.9%). **(B)** Principal component (PC1). **(c)** Mode 2 (13.3%). **(D)** Principal component (PC2). Blue (red) areas indicate negative (positive) values and contours.

over time but maintains a consistent phase alternation, with more persistent peaks compared to PC1.

Eastern El Niño events, such as those in 1965–66, 1972–73, 1982–83 and 1997–98, appear as strong positive peaks in PC2. The overlap between these peaks and the aforementioned events suggests that, in some cases, strong Central El Niños were either preceded or followed by Eastern-type episodes, which may have helped prolong or intensify the Pacific warming phase. However, not all Eastern El Niño events are associated with Central events—some occur independently, with the central Pacific region remaining cool or even neutral.

During negative phases, Eastern La Niña events are evident in the years 1954–55, 1959–60, 1967–68, 1987–88, and 2013–15. This suggests that the Niño 1 + 2 region exhibited below-average temperatures prior to the strong 2015 El Niño. In general, Mode 2 is associated with lower-amplitude variability, capturing intra-seasonal fluctuations or secondary climate patterns (Figure 2d).

Figures 3a,e display the time series of the first two PC1 and PC2, respectively in black, while the gray lines represent the normalized versions of these series. The wavelet power spectra (Figures 3b,f for PC1 and PC2, respectively) illustrate the variation in spectral power across different timescales over the study period. In these panels, the shaded gray areas denote the cone of influence, where edge effects may reduce the reliability of the results. Solid black contours highlight regions of statistically significant power at the 95% confidence level, assessed against a red-noise background spectrum.

Complementarily, the global wavelet spectra (Figures 3c,g) for PC1 and PC2, respectively, represent the average power of all periodicities across the entire time series. In these plots, the dashed horizontal lines indicate the 95% confidence threshold, with peaks above this line corresponding to statistically significant dominant periodicities. The solid gray lines show the smoothed global wavelet power spectra.

Finally, the scale-averaged power time series (Figure 3d for PC1 in the 2–8 year band, and Figure 3h for PC2 in the 1–4 year band) depict the evolution of oscillatory power within specific frequency bands over time. In these graphs, the dashed horizontal lines represent the mean background variance used in significance testing, helping identify periods of enhanced oscillatory activity.

The wavelet transform spectrum of the PC1 time series (Figure 3a) shows strong interannual variability, with pronounced peaks corresponding to major El Niño and La Niña events. The wavelet power spectrum (Morlet) (Figure 3b) reveals the highest energy concentration (in yellow shades) around 2- to 8-year periods, particularly between 1960 and 2000, and again after 2005.

These periods are directly associated with the typical interannual variability of ENSO. In Figure 3c, the global wavelet spectrum displays the average-to-high energy across different period scales for the entire time series. Two well-defined peaks are observed around the 2- to 8-year band, confirming the relevance of ENSO cycles. The dashed line indicates the statistical significance level, showing that variability around these periods is both relevant and statistically significant. In Figure 3d, the mean power in the 2–8 year band reflects the temporal evolution of energy, capturing the strength of ENSO events across decades. A particularly active phase of interannual variability is evident, with peaks occurring during 1955–56, 1964–65, 1972–73, 1982–83, 1987–88, 1997–98, and 2009–10.

The time series of PC2 (Figure 3e) reveals more frequent interannual variability compared to PC1, including peaks that correspond to some Central El Niño events. The wavelet transform applied to PC2 (Figure 3f) highlights the variability of this component at different time scales, with a notable concentration in the 1- to 4-year range, along with other frequent patterns.

The global wavelet spectrum (Figure 3g), summarizing contributions across scales, confirms that the highest power concentration is found in the 1–4 year band. The mean wavelet power (Figure 3h) highlights peaks associated with extreme climate events, such as 1965–66, 1972–73, 1982–83, 1987–88, 1991–92, 1997–98, 2008–09, and 2015–16. These peaks demonstrate that PC2 captures the direct influence of such episodes, which impact not only global climate, but also hydroclimatic variability in the Amazon Basin.

In Figure 3h, the mean power in the 1–4 year band shows the temporal evolution of energy, reflecting the increased frequency of Eastern ENSO events throughout the decades. In summary, PC2 represents dynamics characterized by shorter cycles, with direct links to extreme climate events associated with ENSO. The oscillations in PC2 occur on a higher-frequency scale, with less intense anomalies, predominantly located in the eastern Pacific. This variability has important implications for climate forecasting and for monitoring impacts on Amazonian subregions, since phase shifts in ENSO influence rainfall distribution and the occurrence of droughts and floods in the region.

Based on these analyses—including Pearson correlations, wavelet coherence and phase (Supplementary material)—the identified anomalous modes can be interpreted as distinct physical patterns widely recognized in the literature. Mode 1 represents a Central El Niño pattern, while Mode 2 corresponds to an Eastern El Niño. These results are consistent with the findings of Kao and Yu (2009) and Feng et al. (2020), who identified the existence of two ENSO types: Central Pacific or Modoki El Niño, and Eastern Pacific or Canonical El Niño (Ashok et al., 2007).

In the studies by Kao and Yu (2009), using a method that combined EOF and linear regression, the authors separated and examined the structure, evolution, and possible teleconnections with other regions of the globe due to the two modes. Studies have shown that one mode is characterized by positive SST anomalies confined to the central equatorial Pacific (Kao and Yu, 2009; Feng et al., 2020), while the other is associated with westward propagation of positive SST anomalies in the eastern equatorial Pacific near the coast of South America (Eastern El Niño) (Rasmusson and Carpenter, 1983). This spatial variability implies different convection patterns and atmospheric responses to warming, which can produce different climate teleconnections worldwide (Ashok et al., 2007); however, studies specifically focused on the Amazon region detailing the spatiotemporal variability of these effects remain quite scarce.

3.2 Tropical Atlantic Ocean

The EOF analyses for the Atlantic region (70°W–10°E; 20°S–20°N) for the period from 1950 to 2022 reveal modes of variability that explain 47.2% of the total variance of the data series for Mode 1 and 19.6% for Mode 2 (Figures 4a,c). The first mode shows negative anomalies throughout the ocean basin, with maximum intensity near the Equator, around 30°W, with marked positive events occurring in the years 1969, 1974, 1987, 1998, 2010, and 2020. In contrast, negative

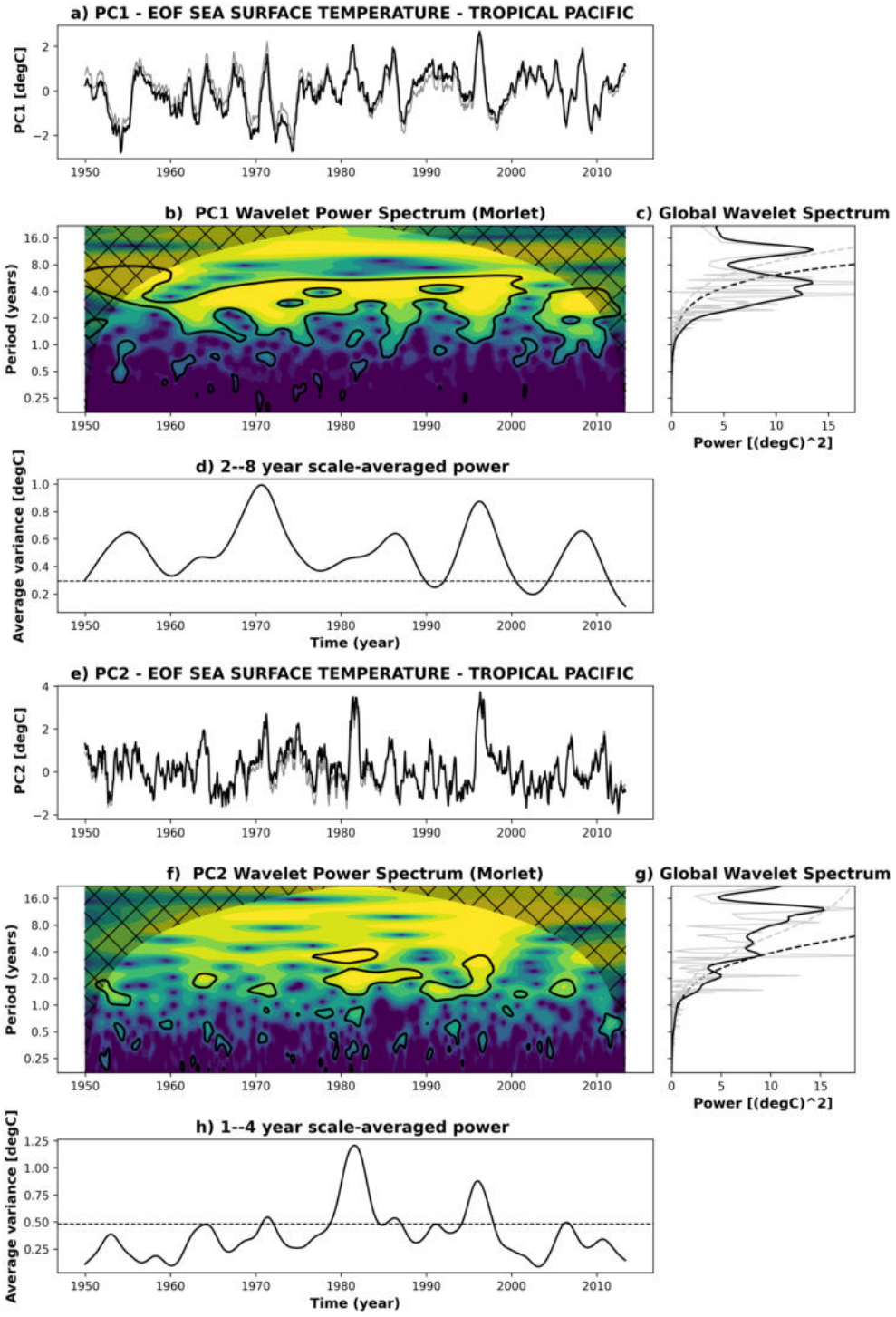

FIGURE 3
Tropical pacific wavelet transform. Tropical Atlantic wavelet transform. **(a)** PC1 time series of the SST in the tropical Atlantic. **(b)** PC1 wavelet spectrum (Morlet). **(c)** Global wavelet spectrum of PC1. **(d)**. Average power on the 1–4 year scale. **(e)** PC2 time series of the SST in the tropical Atlantic. **(f)** PC2 wavelet spectrum (Morlet). **(g)** Global wavelet spectrum of PC2. **(h)** Average power on the 0.5–1 year scale. Continuous contours encompass significant variations at the 95% confidence level, and the curve at Ω is the cone of influence.

events are recorded in 1964, 1967, 1972, 1976, 1993, 1996, 2012, 2018, and 2021 (Figure 4a).

The second mode (EOF 2) (Figure 4c) displays a dipolar pattern, with positive anomalies in the Northern Tropical Atlantic region centered at 15°N, 40°W, and negative anomalies in the Southern Tropical Atlantic, with the most intense area centered at 15°S, 10°W. The main positive peaks are observed in 1957, 1970, 1981, 1996, and 2005, highlighted in the series, while the negative peaks indicate the occurrence of a Negative Dipole, such as the events in 1974, 1989, 1994, and 2018 (Figure 4d).

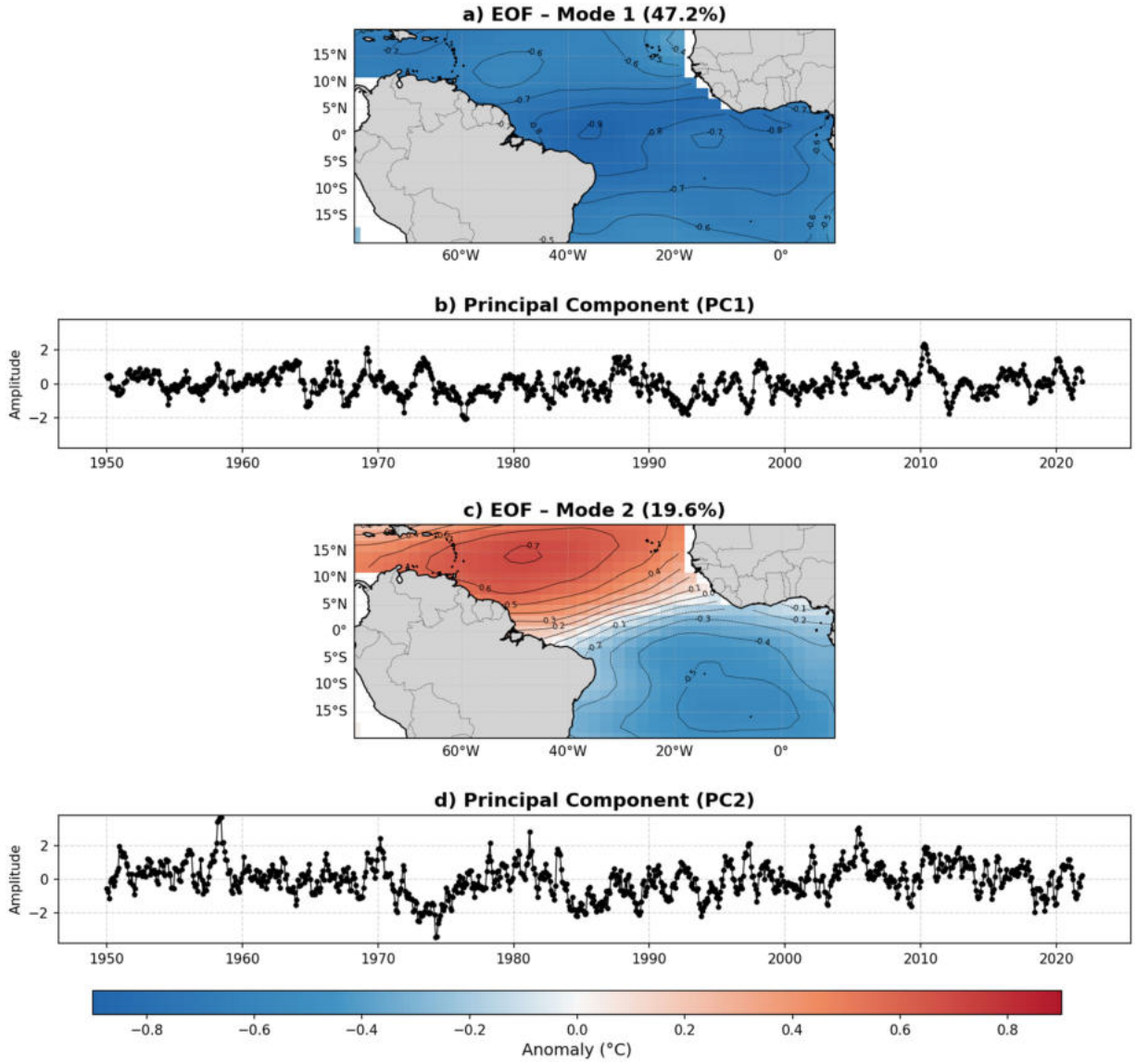

FIGURE 4
Empirical orthogonal function (EOF)—tropical Atlantic. **(a)** Mode 1 (47.2%). **(b)** Principal component (PC1). **(c)** Mode 2 (19.6%). **(d)** Principal component (PC2). Blue (red) areas indicate negative (positive) values and contours.

The Figure 5a presents the original (black line) and normalized (gray line) time series of PC1 for the Atlantic, revealing a peak in the global wavelet spectrum occurring approximately at the 2-4 year scale, with more significant peaks restricted to the 1-4 year scale (Figures 5c,d). Although the signal at this scale is not significant throughout the entire time series, periods of intensified energy for this variability are observed during the 1960s-1970s, 1995-2000 and again around 2010, indicating that interannual variability was more intense during these intervals (Figure 5b). Figure 5c shows a high-power cycle suggesting that these peaks tend to repeat approximately every 20 years, which may indicate a decadal cycle or pattern associated with the Tropical Atlantic.

Figure 5e presents the original (black line) and normalized time series (gray line) of PC2. The panel shows temporal fluctuations of PC2, with intensified variability during certain decades, such as the periods between 1958, 1970-1980 and from 2005 to recent years. These oscillations may indicate specific intervals in which the Tropical Atlantic variability was particularly active (Figure 5f). The wavelet spectral analysis of PC2 reveals a peak in the global wavelet spectrum approximately at the 6-month to 1-year scale (Figure 5f), with energy maxima occurring during 1954-55, 1968-72, 1978-79, 1982-83, 2001-02, 2009-10, 2015-16 and again in 2020 (Figure 5h). This wavelet power spectrum identifies the dominant frequencies in the series over time at intraseasonal scales, indicating a faster oscillation.

A strong pattern of variability is observed at time scales between 8 and 16 years, mainly before the 1970s (Figure 5g). This suggests that PC2 is relevant at multi-annual and decadal time scales, indicating more intense oscillations during some decades, suggesting rapid changes in the Tropical Atlantic SST. This variation is highly irregular, indicating that this temporal band may be influenced by external forcings and rapid interactions.

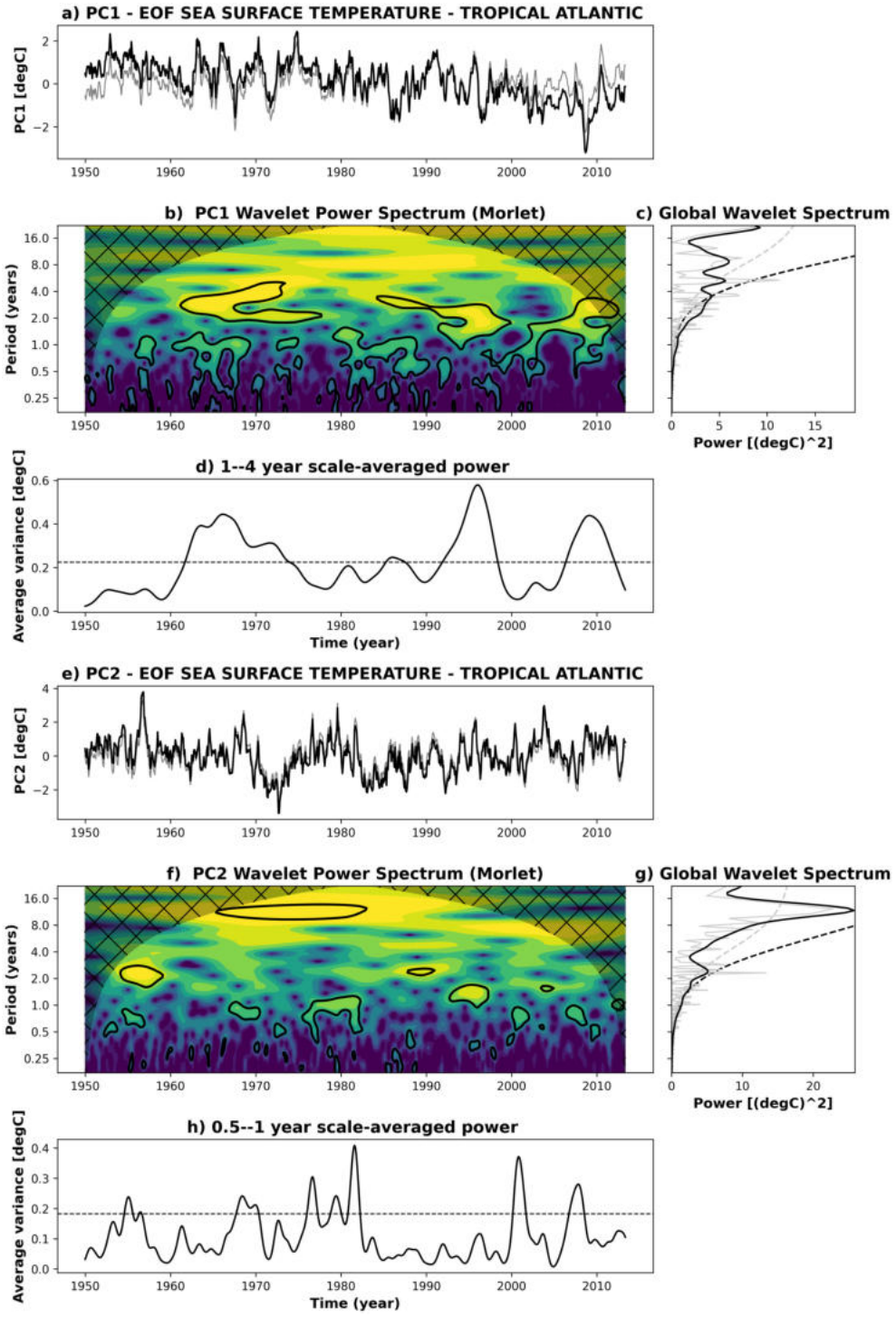

FIGURE 5
Tropical Atlantic wavelet transform. **(a)** PC1 time series of the SST in the tropical Atlantic. **(b)** PC1 wavelet spectrum (Morlet). **(c)** Global wavelet spectrum of PC1. **(d)** Average power on the 1–4 year scale. **(e)** PC2 time series of the SST in the Tropical Atlantic. **(f)** PC2 wavelet spectrum (Morlet). **(g)** Global wavelet spectrum of PC2. **(h)** Average power on the 0.5–1 year scale. Continuous contours encompass significant variations at the 95% confidence level, and the curve at Ω is the cone of influence.

Results from the EOF analysis for the Atlantic region reveal that the first identified mode corresponds to the EAM, while the second mode represents the Atlantic Dipole. Spectral analyses suggest predominantly intraseasonal variability, with cycles between 1 and 4 years for the EAM and between 6 months and 1 year for the Dipole, alongside multiyear and decadal patterns. This irregular variability highlights the Atlantic Oceans influence on SST modulation and its interactions with regional climate.

The EAM impacts the global hydrological cycle by modulating precipitation over parts of South America, whereas the Atlantic Dipole

can intensify or suppress African monsoons and moisture transport toward the Caribbean, southern United States, and Brazil. Both modes affect not only seasonal patterns but also the formation of tropical cyclones, severe drought events, and regional atmospheric dynamics, including shifts in the ITCZ and Walker and Hadley circulations.

3.3 Oceanic patterns and their relationships with dry and wet periods in Amazonia

This section presents the characterization of the study area and the spatial correlation patterns between oceanic climate modes and hydrological variability in the Amazon. Figure 1 highlights the sub-basins of the Amazon Basin, including Japurá, Rio Negro, Jatapu, Trombetas, Jutaí, Purus, Madeira, Tapajós, and Xingu, with the location of the ANA hydrological station in Manaus indicated on the map. This spatial delineation is essential for understanding regional hydrological responses to oceanic oscillations.

Figure 6 presents the spatial correlation patterns between the PDSI and major climate modes in the Tropical Pacific and Atlantic, considering the full time series and the months of January and July. The maps highlight how each mode influences hydrological conditions in different seasons, with blue and red areas indicating positive and negative correlations, respectively. Correlation values above 0.4 and below −0.4 are considered statistically significant at the 95% confidence level, based on the Student's t-test adjusted for autocorrelation in the time series. This analysis allows the identification of areas within the Amazon that are more sensitive to oceanic variability, contributing to the understanding of climatic impacts on extreme hydrological events in the region.

The correlation pattern between the Central El Niño (PC1) and the PDSI across the Amazon sub-basins reveals a spatially homogeneous response. Generally, the Javari, Japurá, Purus, Negro, Trombetas/Uatumã, and Paru/Jari sub-basins exhibit negative correlations with Central El Niño events, indicating these areas experience intensified drought conditions during such events. In

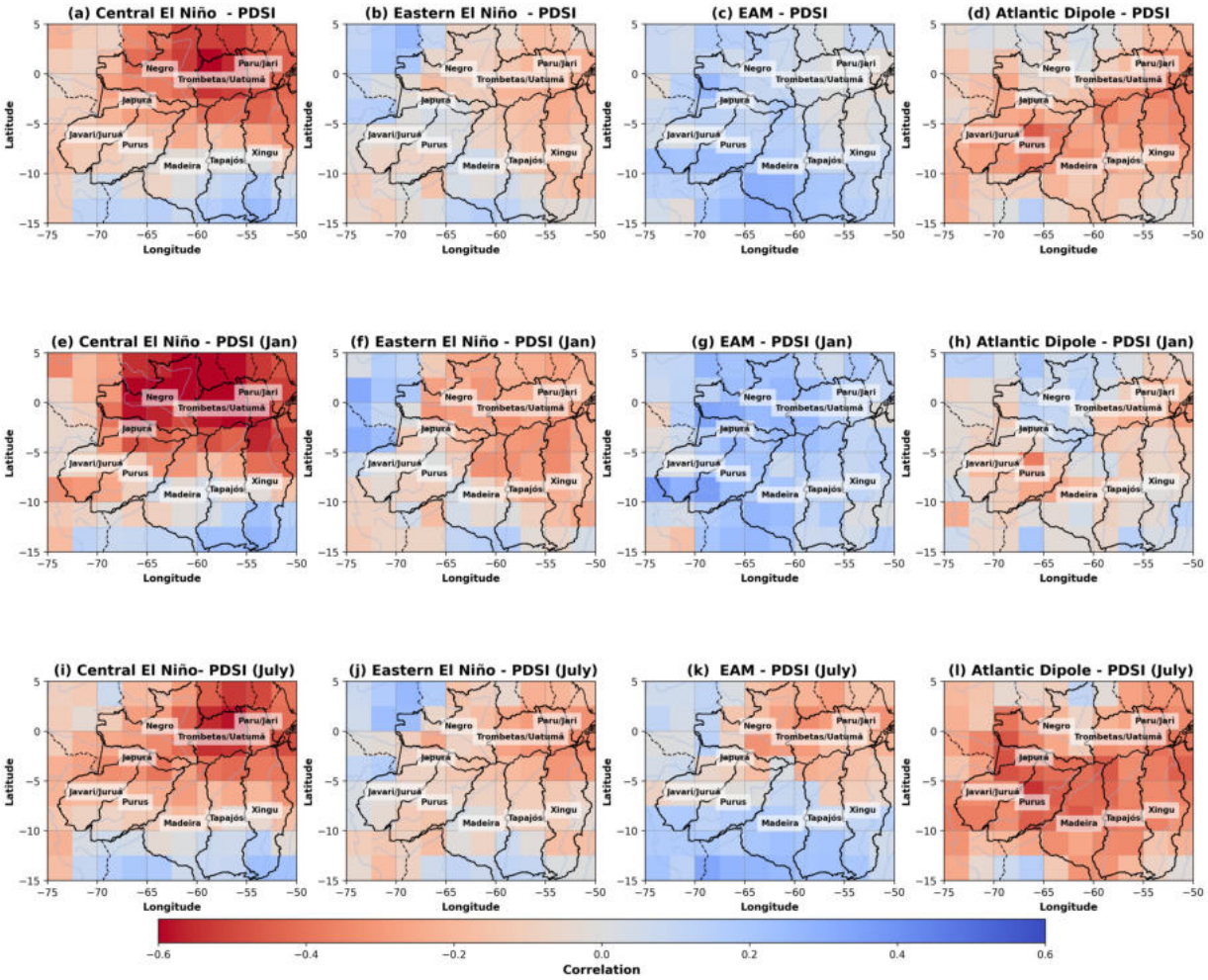

FIGURE 6
Correlation patterns between the Palmer Drought Severity Index (PDSI) and the main oceanic climate modes for the period 1950–2014. **(a)** Central El Niño, **(b)** Eastern El Niño, **(c)** Equatorial Atlantic mode (EAM), and **(d)** Atlantic dipole for the entire analyzed series. For the month of January: **(e)** Central El Niño, **(f)** Eastern El Niño, **(g)** EAM, and **(h)** Atlantic dipole. For the month of July: **(i)** Central El Niño, **(j)** Eastern El Niño, **(k)** EAM, and **(l)** Atlantic dipole. The blue and red regions indicate positive and negative correlations, respectively. Values above 0.4 and below −0.4 are statistically significant at the 95% confidence level, according to Student's *t*-test.

contrast, the southern portion of the Amazon basin shows positive correlations, suggesting enhanced moisture during Central El Niño events, both on the annual mean scale (Figure 6a) and seasonally (Figures 6e,i). The Madeira, Tapajós, and Xingu sub-basins display weaker negative signals in the north and positive correlations in the south, indicating a dipolar impact pattern associated with Central El Niño years.

In the case of the Eastern El Niño, a spatiotemporal variability with more moderate effects and less intense impacts is observed in areas mostly influenced by Central El Niño (Figures 6b,f,j). Furthermore, positive correlations between the Eastern El Niño and PDSI are found in the western portion of the international Amazon, extending to the Upper Rio Negro. This suggests increased moisture during these events in these regions, whereas during Eastern La Niña years, drought conditions may develop in the Upper Rio Negro sub-basin and in parts of northern Peru, Ecuador, and Colombia, with more pronounced effects in January (Figure 6f).

In summary, Central El Niño induces more significant and spatially coherent impacts, with a clear spatial division wherein northern and eastern basins tend to experience severe droughts, while southern basins are less affected or even benefit from increased moisture during these events. Conversely, Eastern El Niño exhibits a more heterogeneous pattern with less intense and more temporally and spatially variable effects. These differences have important implications for climate forecasting and resource management within Amazon sub-basins, highlighting the necessity for regionally tailored approaches considering the specific characteristics of each climate mode.

Regarding the EAM, a positive correlation is observed over most of the Amazon for the full time series (Figure 6c). This indicates that during warm (cold) phases of the EAM, the PDSI tends to show higher (lower) values, favoring wetter (drier) conditions in the region, with a stronger influence observed during the peak rainy season (Figure 6g). The Javari-Juruá, Purus, Madeira, Japurá, and Negro sub-basins are particularly affected by increases (decreases) in moisture.

Conversely, in July (Figure 6k), negative correlations appear in the central and northeastern Amazon basin, including the middle and lower Rio Negro, Trombetas/Uatumã, and Paru-Jari regions (Figure 6c). This suggests that during this period, drier (wetter) conditions prevail in these areas when the Equatorial Atlantic is cold (warm). However, further south, such as in the Purus, Madeira, Tapajós, and Xingu basins, Equatorial Atlantic cooling (warming) may maintain moisture (dry) conditions.

Overall, the EAM exerts a pronounced seasonal effect on the Amazon, especially in January, influencing the quality of the rainy season. In July, it creates drought conditions in the middle and lower Rio Negro, Trombetas-Uatumã, and Paru-Jari during the transition to the dry season.

For the Atlantic Dipole, negative correlations dominate the full series (Figure 6d). This implies that during positive (negative) Dipole events, there is a tendency toward drier (wetter) conditions across nearly the entire Amazon, with stronger impacts in the pre-dry season period (Figure 6l). This effect is particularly marked in the Japurá, Purus, Madeira, Trombetas-Uatumã, Tapajós, Xingu, and Paru-Jari basins, especially in July (Figure 6l). When the positive (negative) Atlantic Dipole pattern develops during the rainy season, the Japurá and Negro sub-basins experience increased (reduced) moisture, whereas other basins display opposite but generally moderate signals (Figure 6h).

These results suggest that Atlantic climate modes exert a seasonal control on the variability of moisture regimes across the Amazon basin. The positive Dipole is consistently associated with droughts, exerting greater influence in northeastern and southern sub-basins, with its impact strongly modulated by occurrence in the months preceding the dry season, acting as an amplifier of drought conditions. Conversely, the warm (cold) phase of the EAM is associated with enhanced (reduced) moisture over much of the Amazon, particularly during the rainy season, but may contribute to drought conditions in the middle and lower Rio Negro, Trombetas/Uatumã, and Paru-Jari regions during the transition to the dry season. Understanding this seasonality is crucial for climate prediction and water resource management in the region, emphasizing the need for regionally adapted strategies to mitigate the seasonal impacts of each climate mode.

3.4 Extreme events in Central Amazonia

The graph presented in Figure 7a provides a detailed view of the variability in water levels of the Rio Negro at the Manaus gauge station over the period from 1950 to 2024, highlighting extreme flood and drought events. The historical time series reveals well-defined patterns, characterized by pronounced annual oscillations with distinct peaks and troughs, as well as an increase in the frequency and intensity of extreme events in recent decades.

The most intense flood events, highlighted in blue, occurred in the years 1976, 2009, 2012, 2015, 2019, 2021, and 2022, whereas the most severe droughts, marked in red, include the years 1958, 1963, 1995, 1997, 2005, 2010, 2023, and potentially 2024.

The analysis of extreme flood events compared to the historical climatology shows that the most critical years exhibited water levels significantly above the long-term average, with peak stages occurring between May and July (Figure 7b). The 2022 event stands out as one of the most intense, surpassing all previously recorded floods. Following the peak months, water levels sharply decline from August onwards, gradually returning to climatological mean values. The recurrence of these floods suggests an increase in the magnitude of inundation events, which may be linked to large-scale climatic drivers such as Pacific and Atlantic oceanic oscillations.

Conversely, the analysis of extreme drought events indicates a pronounced reduction in river levels, especially starting in August, reaching the lowest values between October and November (Figure 7c). The years 2023 and 2024 exhibit exceptionally low water levels, positioning the 2024 drought among the most severe in the historical record. The progressive intensification of droughts points to a worsening hydrological condition in the region, underscoring the necessity to investigate the influence of oceanic modes, including El Niño/La Niña and Tropical Atlantic anomalies, on the hydrological variability of the Amazon basin.

Based on these data, the selected years for further analysis consider both extreme flood and drought events. This approach enables the exploration of possible links between these critical periods and the prevailing oceanic conditions on annual and seasonal timescales.

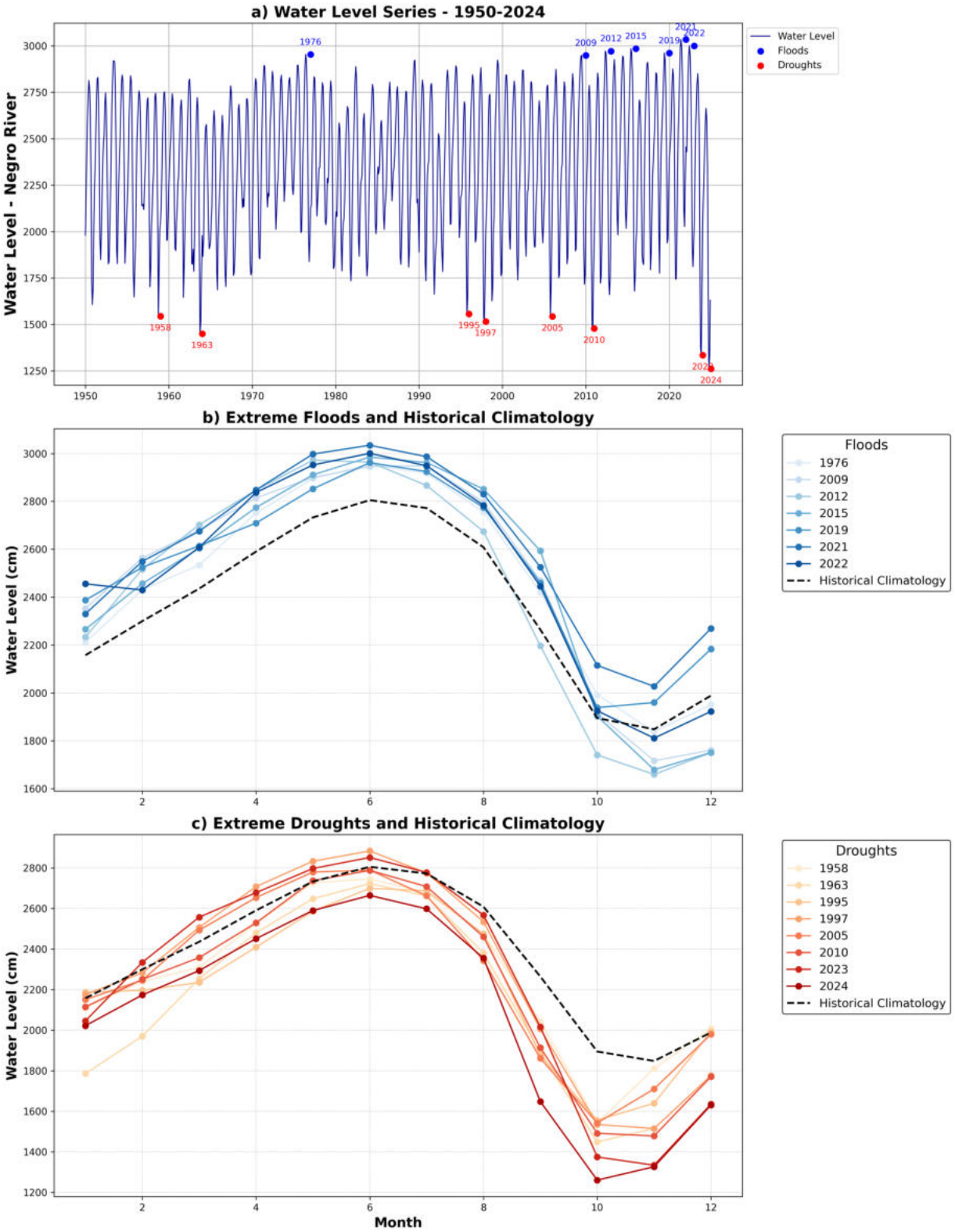

FIGURE 7
Evolution of water levels in the Rio Negro at the Manaus station between 1950 and 2024. **(a)** River level time series—the historical series shows the annual variation of the Negro River level, highlighting years of extreme floods (blue points) and extreme droughts (red points). **(b)** Extreme floods and historical climatology—the seasonal variation of the river level for extreme flood years (blue-violet lines) compared to the historical climatology (dashed black line). **(c)** Extreme droughts and historical climatology—the seasonal variation of the river level for extreme drought years (orange-red lines) compared to the historical climatology (dashed black line).

3.5 The flood events of 1976, 2009, 2012, 2015, 2019, 2021, and 2022

The graphs presented in Figure 8 depict the temporal evolution of anomalies in the primary tropical oceanic modes—Central El Niño, Eastern El Niño, EAM, and Atlantic Dipole—across the months corresponding to the extreme flood years in the Amazon basin: 1976, 2009, 2012, 2015, 2019, and 2021.

Each graph in Figure 8 represents a specific flood year, highlighting how these oceanic phenomena fluctuated amid the region's hydrological conditions. For the 1976 flood (Figure 8a), a predominant influence of a Central La Niña (red) is observed, with persistent negative anomalies from January to August, coinciding with the rising flood stage in Central Amazonia. Concurrently, an Eastern El Niño (yellow) developed, characterized by positive anomalies in the Niño 1 + 2 region, while negative anomalies persisted in the central Pacific throughout the year. The negative correlation between these two tropical Pacific modes and the Palmer.

The PDSI indicates increased soil moisture during the region's rainy season. The EAM (green) remained in a positive phase throughout the year, which, as shown by the correlation analysis, supported a regime of persistently higher humidity. The Atlantic Dipole (blue) exhibited a negative phase during the first half of the year and a positive phase during the second. Given its negative correlation with the PDSI, this configuration favors wetter conditions during the first semester. Collectively, the 1976 flood was driven by the influence of a Central La Niña and a negative Atlantic Dipole in the first half of the year, along with a positive-phase EAM and a persistent Eastern El Niño throughout the year. These oceanic patterns promoted enhanced moisture availability, contributing to the intensification of the extreme event in the region.

The oceanic anomaly pattern during the 2009 flood exhibited similarities to 1976 (Figure 8b), but with notable differences. In 2009, the Atlantic Dipole displayed a stronger negative phase in the first semester, while the Central La Niña and Eastern El Niño were less intense compared to 1976. These variations may have played a crucial role in amplifying the 2009 flood, which exceeded the magnitude of the 1976 event.

In 2012 (Figure 8c), a combined influence of a Central La Niña and an Eastern El Niño is again observed, similar to previously analyzed years. However, both the EAM and the Atlantic Dipole exhibited strong positive phases throughout the year. This pattern suggests that the warm EAM, due to its positive correlation with the PDSI, contributed to maintaining elevated moisture levels during the entire period, mitigating the usual drying effects associated with a positive Dipole phase.

In 2015 (Figure 8d), an intense Eastern La Niña combined with a Central El Niño (red) during the first semester is evident. The EAM remained in a positive phase, while the Atlantic Dipole showed a negative phase in the first semester. This combination favors increased moisture in the region, especially during this period. In 2019 (Figure 8e), a similar pattern in tropical SST anomalies is identified,

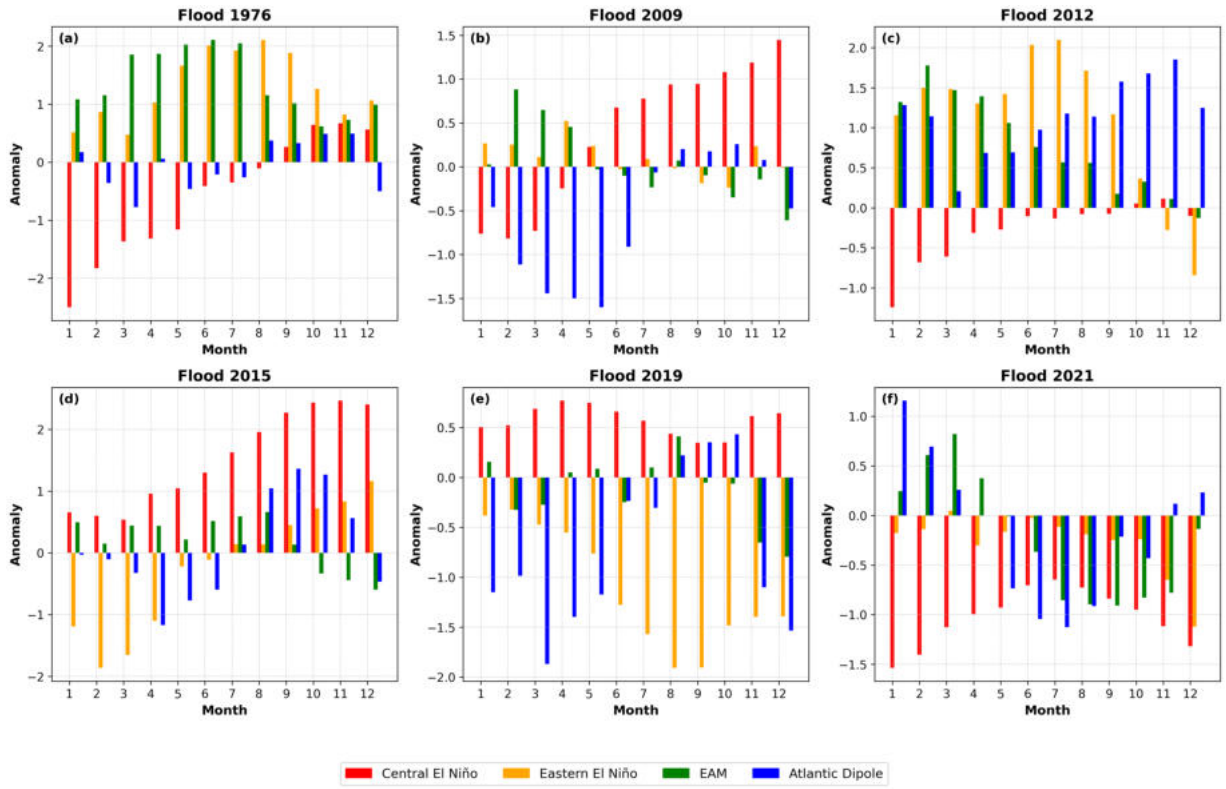

FIGURE 8
Monthly anomalies of the principal components (PCs) associated with climate patterns during the years of extreme floods in the Amazon for the years **(a)** 1976, **(b)** 2009, **(c)** 2012, **(d)** 2015, **(e)** 2019, and **(f)** 2021. The bars represent the normalized anomalies for Central El Niño (red), Eastern El Niño (orange), Equatorial Atlantic Mode (EAM) (green) and Atlantic Dipole (blue).

although the negative Atlantic Dipole exhibited a more pronounced influence, further intensifying moisture conditions in the Amazon.

The extreme 2021 (Figure 8f) event was characterized by a strong influence of an intense Central La Niña combined with a weaker Eastern La Niña. Additionally, the EAM maintained a positive phase throughout the year, contributing to persistent moisture during this period.

These results suggest that extreme floods in the Amazon are strongly associated with the presence of a Central La Niña, a positive EAM, and a negative phase of the Atlantic Dipole, especially during the first semester. Such oceanic configurations favor a sustained increase in regional moisture, thereby intensifying hydrological extreme events.

3.6 Droughts of 1958, 1963, 1995, 1997, 2005, and 2010

The analysis of tropical oceanic modes contributions during drought years in Central Amazonia reveals a predominant influence of El Niño events. These events may be confined to the first semester, as observed in 1995 (Figure 9c), 2005 (Figure 9e), and 2010 (Figure 9f), persist throughout the entire year, as in 1958 (Figure 9a), or progressively intensify, as in 1963 (Figure 9b) and 1997 (Figure 9d). These patterns indicate that variability in Pacific SST anomalies plays a key role in moisture reduction and drought intensification in the region. This influence aligns with the negative correlations identified in the PDSI analysis, highlighting the strong linkage between El Niño events and decreased moisture availability in Central Amazonia.

In drought years where El Niño's influence was more restricted to the first semester, such as 1995, 2005, and 2010, a positive phase of the Atlantic Dipole is observed either throughout the year (Figures 9e,f) or during the second semester (Figure 9c). Given the negative correlation between the Atlantic Dipole and the PDSI, this pattern corresponds to a significant reduction in moisture during this period, thereby exacerbating drought conditions in the Amazon. This mechanism compounds the drought effects already established at the end of the rainy season due to El Niño's influence.

For El Niño events persisting throughout the year, such as in 1958 (Figure 9a), the positive Atlantic Dipole also played a crucial role in intensifying the drought by prolonging its duration and expanding the spatial extent of impacted areas. Correlation analyses with the PDSI demonstrate that El Niño primarily affects the central and northern regions, while the positive Atlantic Dipole exerts greater influence over central, southeastern, and southern areas.

In years when El Niño events progressively intensified, such as in 1963 and 1997, a simultaneous evolution of a positive Eastern Pacific El Niño was also observed, resulting in large-scale events with gradually increasing impacts throughout the year. In the second half of the year, the action of the EAM in its negative phase suggests a reduction in moisture during the period preceding the dry season in the Amazon. This is supported by the negative correlation between its July signal and the PDSI (Figures 9b,d). This pattern indicates that the negative phase of the EAM can amplify

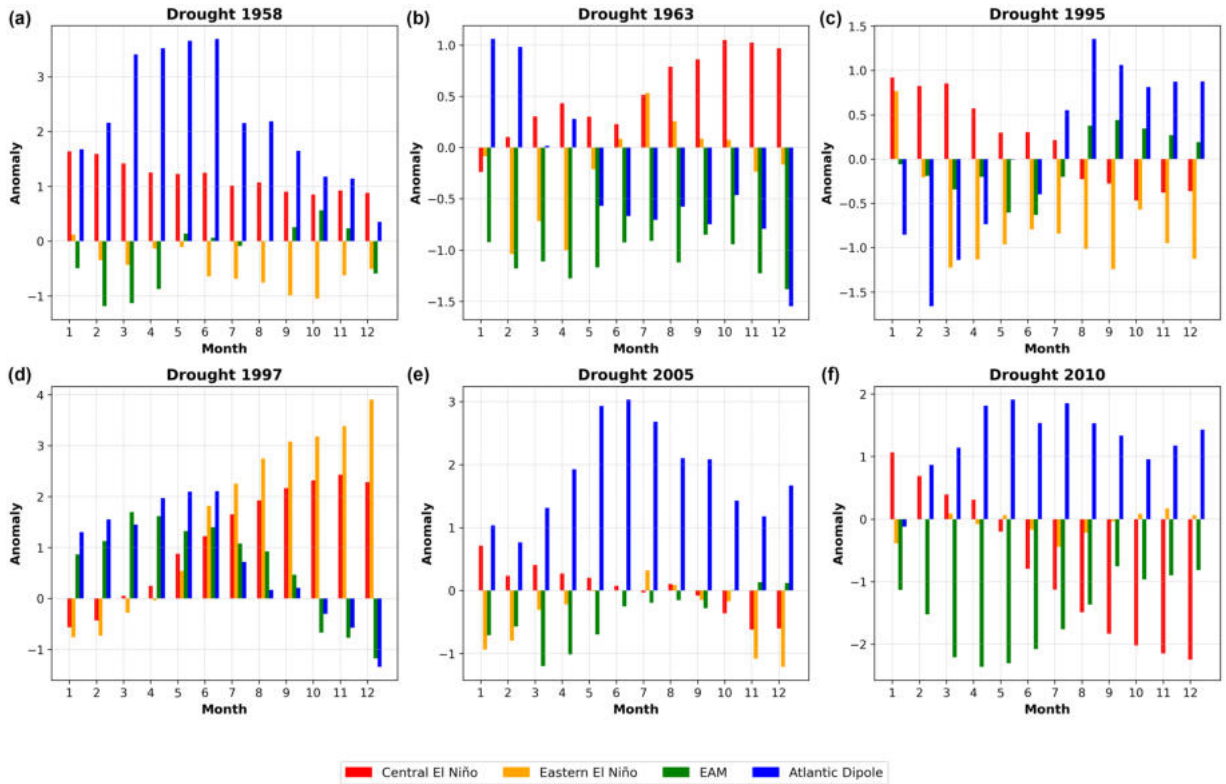

FIGURE 9
Monthly anomalies of the principal components (PCs) associated with climate patterns during the years of extreme droughts in the Amazon for the years **(a)** 1958, **(b)** 1963, **(c)** 1995, **(d)** 1997, **(e)** 2005, and **(f)** 2010. The bars represent the normalized anomalies for El Niño Central (red), El Niño Eastern (orange), Equatorial Atlantic Mode (EAM) (green) and Atlantic Dipole (blue).

drought effects by significantly influencing the transition between seasons and intensifying hydrological deficits in the region.

4 Discussion

This study highlights the spatial and temporal correlations between oceanic climate modes and hydroclimatic extremes in the Amazon sub-basins. The analysis identified which sub-basins respond most strongly to Central and Eastern Pacific El Niño events, as well as to the Atlantic Dipole and EAM phases, revealing pronounced spatial and temporal heterogeneity in hydroclimatic responses.

The Central El Niño emerged as the main driver of prolonged droughts, exerting strong and widespread impacts on the northern and central sub-basins, including the Japurá, Negro, Trombetas-Uatumã, and Paru-Jari basins. The northern and eastern sub-basins (e.g., Javari and Purus) experienced severe droughts, while the southern sub-basins experienced increased humidity. In contrast, the Eastern El Niño produced moderate and spatially diffuse effects, particularly affecting the Upper Rio Negro sub-basin.

The EAM modulates seasonal variability, with warm phases generally increasing precipitation during the rainy season, while cool phases during the transition to the dry season induce localized drought in the Middle and Lower Negro, Trombetas-Uatumã, and Paru-Jari sub-basins. Sub-basins such as the Purus, Madeira, Juruá, and Tapajós maintain relatively high humidity throughout the year. Positive Atlantic Dipole phases consistently intensify drought conditions at the beginning of the dry season, particularly in Japurá, Purus, Madeira, Trombetas-Uatumã, and Paru-Jari.

The most extreme flood events were associated with oceanic configurations that increased regional humidity and amplified hydrological extremes. For example, the 2009 and 2019 floods coincided with a negative Atlantic Dipole during the first half of the year. The 1976, 2012, and 2021 floods occurred under the combined influence of Central La Niña and Eastern El Niño conditions, while the 2015 flood was associated with Eastern La Niña. Notably, in all years analyzed except 2009, the EAM was in its warm phase during this period.

Severe droughts occurred as single events; however, their duration and persistence were strongly modulated by the dynamic variability of the tropical Atlantic. In years where the influence of Central El Niño was limited to the first half of the year (e.g., 2010), subsequent Atlantic conditions—particularly the cool phase of the EAM—further suppressed moisture availability in the second half. In years with prolonged El Niño conditions (e.g., 1997), the concurrent Eastern El Niño contributed to prolonged droughts across the basin, amplifying their severity. In 1995, the Central El Niño phenomenon persisted in the first half of the year and the positive Atlantic Dipole in the second half of the year, further intensifying drought conditions. In 1958 and 2005, the positive Atlantic Dipole remained active throughout the year, exacerbating dry season deficits, particularly in the southern Amazon.

In summary, these results highlight the complementary roles of the Pacific and Atlantic oceans in shaping hydroclimatic extremes in the Amazon Basin. The study demonstrates pronounced spatial heterogeneity and temporal variability in sub-basin responses, offering crucial insights for climate monitoring, early warning systems, and adaptation strategies.

Data availability statement

The original contributions presented in the study are included in the article, further inquiries can be directed to the corresponding author/s.

Author contributions

RS: Writing – original draft, Writing – review & editing. PF: Writing – original draft, Writing – review & editing.

Funding

The author(s) declare that financial support was received for the research and/or publication of this article. This work was supported by a postdoctoral fellowship from CAPES – INCT for the Environmental Value of the Amazon – VALAMB. The APC payment was covered by INCT VALAMB.

Acknowledgments

RS thanks the National Institute for Research in the Amazon (INPA) Institutional Training Program (PCI) for a post-doctoral fellowship (Process 301400/2023-7). PF thanks the INPA Institutional Research Program (PPI) (PRJ15.125), the Brazilian Research Network on Climate Change (FINEP/Rede CLIMA) (Process 01.13.0353-00), the National Council for Scientific and Technological Development (CNPq) (Processes 312450/2021-4; 406941/2022-0), the Research Support Foundation of Amazonas state (FAPEAM) (Process 01.02.016301.02529/2024-87) and the Coordination for the Improvement of Higher Education Personnel (CAPES) (Process 88887.95454/2024-00). We thank Sarah Helfand for conversations during preparation of the manuscript.

Conflict of interest

The authors declare that the research was conducted in the absence of any commercial or financial relationships that could be construed as a potential conflict of interest.

Generative AI statement

The authors declare that no Gen AI was used in the creation of this manuscript.

Any alternative text (alt text) provided alongside figures in this article has been generated by Frontiers with the support of artificial intelligence and reasonable efforts have been made to ensure accuracy, including review by the authors wherever possible. If you identify any issues, please contact us.

Publisher's note

References

Aceituno, P. (1988). On the functioning of the southern oscillation in the south American sector. Part I: surface climate. *Mon. Weather Rev.* 116, 505–524. doi: 10.1175/1520-0493(1988)116<0505:OTFOTS>2.0.CO;2

Araújo, R. G., Andreoli, R. V., Candido, L. A., Kayano, M. T., and Souza, R. A. F. (2013). Influence of El Niño-southern oscillation and equatorial Atlantic on rainfall over northern and northeastern regions of South America. *Acta Amazon.* 43, 469–480. doi: 10.1590/S0044-59672013000400009

Ashok, K., Behera, S. K., Rao, S. A., Weng, H., and Yamagata, T. (2007). El Niño Modoki and its possible teleconnection. *J. Geophys. Res. Oceans* 112:art. C11007. doi: 10.1029/2006JC003798

Bjerknes, J. (1966). A possible response of the atmospheric Hadley circulation to equatorial anomalies of ocean temperature. *Tellus A* 18, 820–829. doi: 10.3402/tellusa.v18i4.9712

Bjerknes, J. (1969). Atmospheric teleconnections from the equatorial Pacific. *Mon. Weather Rev.* 97, 163–172. doi: 10.1175/1520-0493(1969)097<0163:ATFTEP>2.3.CO;2

Cox, P. M., Harris, P. P., Huntingford, C., Betts, R. A., Collins, M., Jones, C. D., et al. (2008). Increasing risk of Amazonian drought due to decreasing aerosol pollution. *Nature* 453, 212–215. doi: 10.1038/nature06960

Czaja, A., Van der Vaart, P., and Marshall, J. B. (2002). A diagnostic study of the role of remote forcing in tropical Atlantic variability. *J. Clim.* 15, 3280–3290. doi: 10.1175/1520-0442(2002)015<3280:ADSOTR>2.0.CO;2

Enfield, D. B., and Mayer, D. A. (1997). Tropical Atlantic Sea surface temperature variability and its relation to El Niño-southern oscillation. *J. Geophys. Res. Oceans* 102, 929–945. doi: 10.1029/96JC03296

Espinoza, J. C., Marengo, J. A., Schongart, J., and Jimenez, J. C. (2022). The new historical flood of 2021 in the Amazon River compared to major floods of the 21st century: atmospheric features in the context of the intensification of floods. *Weather Clim. Extremes* 35:100406. doi: 10.1016/j.wace.2021.100406

Espinoza, J. C., Ronchail, J., Marengo, J. A., and Segura, H. (2019). Contrasting north–south changes in Amazon wet-day and dry-day frequency and related atmospheric features (1981–2017). *Clim. Dyn.* 52, 5413–5430. doi: 10.1007/s00382-018-4462-2

Feldpausch, T. R., Lloyd, J., Lewis, S. L., Brienen, R. J. W., Gloor, E., Monteagudo, A., et al. (2012). The Amazon forest biomass, climate and fire interactions. *Biogeosciences.* 9, 3381–3403. doi: 10.5194/bg-9-3381-2012

Feng, Y., Chen, X., and Tung, K. K. (2020). ENSO diversity and the recent appearance of Central Pacific ENSO. *Clim. Dyn.* 54, 413–433. doi: 10.1007/s00382-019-05005-7

Garcia, B. N., Libonati, R., and Nunes, A. M. B. (2018). Extreme drought events over the Amazon Basin: the perspective from the reconstruction of south American hydroclimate. *Water* 10:1594. doi: 10.3390/w10111594

Giannini, A., Kushnir, Y., and Cane, M. A. (2000). Interannual variability of Caribbean rainfall, ENSO, and the Atlantic Ocean. *J. Clim.* 13, 297–311. doi: 10.1175/1520-0442(2000)013<0297:IVOCRE>2.0.CO;2

Giannini, A., Saravanan, R., and Chang, P. (2004). The preconditioning role of tropical Atlantic variability in the development of the ENSO teleconnection: implications for the prediction of Nordeste rainfall. *Clim. Dyn.* 22, 839–855. doi: 10.1007/s00382-004-0420-2

Grimm, A. M., Ferraz, S. E. T., and Gomes, J. (1998). Precipitation anomalies in southern Brazil associated with El Niño and La Niña events. *J. Clim.* 11, 2863–2880. doi: 10.1175/1520-0442(1998)011<2863:PAISBA>2.0.CO;2

Grimm, A. M., and Zilli, M. T. (2009). Interannual variability and seasonal evolution of summer monsoon rainfall in South America. *J. Clim.* 22, 2257–2275. doi: 10.1175/2008JCLI2345.1

Guan, B., and Nigam, S. (2009). Analysis of Atlantic SST variability factoring interbasin links and the secular trend: clarified structure of the Atlantic multidecenal oscillation. *J. Clim.* 22, 4228–4240. doi: 10.1175/2009JCLI2921.1

Handoh, I. C., Matthews, A. J., Bigg, G. R., and Stevens, D. P. (2006). Interannual variability of the tropical Atlantic independent of and associated with ENSO: part I. The North tropical Atlantic. *Int. J. Climatol.* 26, 1937–1956. doi: 10.1002/joc.1343

Kao, H. Y., and Yu, J. Y. (2009). Contrasting eastern-Pacific and central-Pacific types of ENSO. *J. Clim.* 22, 615–632. doi: 10.1175/2008JCLI2309.1

Kay, G., Dunstone, N. J., Smith, D. M., Betts, R. A., Cunningham, C., and Scaife, A. A. (2022). Assessing the chance of unprecedented dry conditions over North Brazil during El Niño events. *Environ. Res. Lett.* 17:064016. doi: 10.1088/1748-9326/ac6df9

Kayano, M. T., and Andreoli, R. V. (2006). Relationships between rainfall anomalies over northeastern Brazil and the El Niño-southern oscillation. *J. Geophys. Res. Atmos.* 111:art. D13101. doi: 10.1029/2005JD006142

Latif, M., Semenov, V. A., and Park, W. (2015). Super El Niños in response to global warming in a climate model. *Clim. Chang.* 132, 489–500. doi: 10.1007/s10584-015-1439-6

Lee, S. K., Enfield, D. B., and Wang, C. (2008). Why do some El Niños have no impact on tropical North Atlantic SST? *Geophys. Res. Lett.* 35:art. L16705. doi: 10.1029/2008GL034734

Liebmann, B., and Marengo, J. A. (2001). Interannual variability of the rainy season and rainfall in the Brazilian Amazon Basin. *J. Clim.* 14, 4308–4318. doi: 10.1175/1520-0442(2001)014<4308:IVOTRS>2.0.CO;2

Marengo, J. A. (2004). Interdecadal variability and trends of rainfall across the Amazon basin. *Theor. Appl. Climatol.* 78, 79–96. doi: 10.1007/s00704-004-0045-8

Marengo, J. A. (2005). Characteristics and spatio-temporal variability of the Amazon River basin water budget. *Clim. Dyn.* 24, 11–22. doi: 10.1007/s00382-004-0461-6

Marengo, J. A. (2006) On the hydrological cycle of the Amazon basin; a historical review and current state-of-the-art Rev. Bras. Meteorol., 21, 1–19. Available online at: https://www.researchgate.net/publication/228647135_On_the_hydrological_cycle_of_the_Amazon_Basin_A_historical_review_and_current_state-of-the-art

Marengo, J. A., and Hastenrath, S. (1993). Case studies of extreme climatic events in the Amazon Basin. *J. Clim.* 6, 617–627. doi: 10.1175/1520-0442(1993)006<0617:CSOECE>2.0.CO;2

Marengo, J. A., Nobre, C. A., Tomasella, J., Oyama, M. D., de Oliveira, G. S., Oliveira, R., et al. (2008). The drought of Amazonia in 2005. *J. Clim.* 21, 495–516. doi: 10.1175/2007JCLI1600.1

North, G. R., Bell, T. L., Cahalan, R. F., and Moeng, F. J. (1982). Sampling errors in the estimation of empirical orthogonal functions. *Mon. Weather Rev.* 110, 699–706. Available at: https://journals.ametsoc.org/view/journals/mwre/110/7/1520-0493_1982_110_0699_seiteo_2_0_co_2.pdf

Price, J., Warren, R., Forstenhäusler, N., Wallace, C., Jenkins, R., Osborn, T. J., et al. (2022). Quantification of meteorological drought risks between 1.5 C and 4 C of global warming in six countries. *Clim. Chang.* 174:art. 12. doi: 10.1007/s10584-022-03359-2

Rasmusson, E. M., and Carpenter, T. H. (1983). The relationship between eastern equatorial Pacific Sea surface temperatures and rainfall over India and Sri Lanka. *Mon. Weather Rev.* 111, 517–528. doi: 10.1175/1520-0493(1983)111<0517:TRBEEP>2.0.CO;2

Ronchail, J., Cochonneau, G., Molinier, M., Guyot, J. L., Chaves, A. G. M., Guimarães, V., et al. (2002). Interannual rainfall variability in the Amazon Basin and sea-surface temperatures in the equatorial Pacific and the tropical Atlantic oceans. *Int. J. Climatol.* 22, 1663–1686. doi: 10.1002/joc.815

Ronchail, J., and Gallaire, R. (2006). ENSO and rainfall along the Zongo valley (Bolivia) from the Altiplano to the Amazon basin. *Int. J. Climatol.* 26, 1223–1236. doi: 10.1002/joc.1296

Ropelewski, C. F., and Halpert, M. S. (1989). Precipitation patterns associated with the high index phase of the southern oscillation. *J. Clim.* 2, 268–284. doi: 10.1175/1520-0442(1989)002<0268:PPAWTH>2.0.CO;2

Salati, E., and Vose, P. B. (1984). Amazon Basin: a system in equilibrium. *Science* 225, 129–138. doi: 10.1126/science.225.4658.129

Silva, M. V., Paris, A., Calmant, S., Cândido, L. A., and da Silva, J. S. (2018). Relationships between Pacific and Atlantic Ocean Sea surface temperatures and water levels from satellite altimetry data in the Amazon rivers. *RBRH* 23:e32. doi: 10.1590/2318-0331.231820170148

Sioli, H. (1984). "The Amazon and its main affluents: hydrography, morphology of the river courses, and river types" in The Amazon: limnology and landscape ecology of a mighty tropical river and its basin. ed. H. Sioli (Dordrecht: Springer), 127–165.

Smith, T. M., Reynolds, R. W., Peterson, T. C., and Lawrimore, J. (2008). Improvements to NOAA'S historical merged land-ocean surface temperature analysis (1880-2006). *J. Clim.* 21, 2283–2296. doi: 10.1175/2007JCLI2100.1

Takahashi, K., Montecinos, A., Goubanova, K., and Dewitte, B. (2011). ENSO regimes: reinterpreting the canonical and modoki El Niño. *Geophys. Res. Lett.* 38:art. L10704. doi: 10.1029/2011gl047364

Torrence, C., and Compo, G. P. (1998). A practical guide to wavelet analysis. *Bull. Am. Meteorol. Soc.* 79, 61–78. doi: 10.1175/1520-0477(1998)079<0061:APGTWA>2.0.CO;2

Wells, N., Goddard, S., and Hayes, M. J. (2004). A self-calibrating palmer drought severity index. *J. Clim.* 17, 2335–2351. doi: 10.1175/1520-0442(2004)017<2335:ASPDSI>2.0.CO;2

Yoon, J. H., and Zeng, N. (2010). An Atlantic influence on Amazon rainfall. *Clim. Dyn.* 34, 249–264. doi: 10.1007/s00382-009-0551-6

Zeng, N., Yoon, J.-H., Marengo, J. A., Subramaniam, A., Nobre, C. A., Mariotti, A., et al. (2008). Causes and impacts of the 2005 Amazon drought. *Environ. Res. Lett.* 3:014002. doi: 10.1088/1748-9326/3/1/014002

Zhao, Y., and Capotondi, A. (2024). The role of the tropical Atlantic in tropical Pacific climate variability. *NPJ Clim. Atmos. Sci.* 7:140. doi: 10.1038/s41612-024-00677-3